Journal of Glaciology



Article

Cite this article: Larsen SH, Ahlstrøm AP, Karlsson NB, Kusk A, Langen PL, Hvidberg CS (2023). Outlet glacier flow response to surface melt: based on analysis of a high-resolution satellite data set. *Journal of Glaciology* **69**(276), 1047–1055. https://doi.org/10.1017/jog.2022.124

Received: 3 January 2022
Revised: 12 December 2022
Accepted: 16 December 2022
First published online: 16 January 2023

Keywords:
Ice dynamics; ice streams; subglacial processes

Author for correspondence:
Signe H. Larsen, E-mail: shl@geus.dk

© The Author(s), 2023. Published by Cambridge University Press on behalf of The International Glaciological Society. This is an Open Access article, distributed under the terms of the Creative Commons Attribution licence (http://creativecommons.org/licenses/by/4.0/), which permits unrestricted re-use, distribution and reproduction, provided the original article is properly cited.

cambridge.org/jog

Outlet glacier flow response to surface melt: based on analysis of a high-resolution satellite data set

Signe H. Larsen[1], Andreas P. Ahlstrøm[1], Nanna B. Karlsson[1], Anders Kusk[2], Peter L. Langen[3] and Christine S. Hvidberg[4]

[1]Department of Glaciology and Climate, Geological Survey of Denmark and Greenland (GEUS), Copenhagen, Denmark; [2]National Space Institute, Technical University of Denmark, Kongens Lyngby, Denmark; [3]Department of Environmental Science, iClimate, Aarhus University, Roskilde, Denmark and [4]Niels Bohr Institute, University of Copenhagen, Copenhagen, Denmark

The dynamics of the Greenland Ice Sheet are affected by surface meltwater reaching the base of the ice, altering ice contact with the bedrock. Lack of understanding of this evolution hampers the ability to predict the effects of increasing temperatures on the Greenland Ice Sheet mass balance. Here we present a unique high-resolution study of ice velocity response to surface melting based on data from a COSMO-SkyMed satellite campaign over Upernavik Isstrøm (Northwest Greenland) for two months around the end of the 2014 melt season. We show that the velocity variations, due to both short-term (days) and seasonal variations in surface melt rates, are increasing in relative strength farther from the glacier terminus. Furthermore, we observe how ice dynamic response to frontal retreat, reaching several kilometres inland, can obscure the meltwater-induced velocity change close to the terminus. Future studies should consider the flow velocity dependence on the distance to the terminus, and local geometry, to distinguish subglacial hydrologic system changes from frontal processes and local basal conditions.

1. Introduction

The mass loss of the Greenland Ice Sheet has increased over the past decades as a response to the warming global climate (The IMBIE Team, 2020). Approximately 66 % of this mass loss is attributed to dynamic mass loss from marine-terminating glaciers (for 1972–2018, see Mouginot and others, 2019). The ability to predict future changes on timescales that are relevant for present-day society is hampered in part by the lack of understanding of the non-linear response of glacier flow to climate change, including how surface meltwater affects glacier flow (Catania and others, 2020).

Around 80 % or more of the flow of marine-terminating glaciers can be attributed to sliding over the bedrock (Cuffey and Paterson, 2010). Water is constantly present in the areas where ice is sliding, mainly due to frictional heat (Karlsson and others, 2021). During the melt season, meltwater on the surface will form pathways to the base of the ice, and most of the surface meltwater drains to the fjords via the ice/bed interface (van der Veen and others, 2011). The influx of water at the base reduces the ice/bed contact and thereby increases glacier slip (e.g. Bartholomew and others, 2010; Sole and others, 2013; Rathmann and others, 2017). Sustained input of water cause cavities and channels to form (e.g. Hoffman and Price, 2014). Continued evolution of the drainage system can lead to efficient drainage of distributed subglacial water, thus leaving the water pressure at the bed lower than before the initiation of surface melt, and the effect of this can be observed as glaciers slow-down to below the winter level (e.g. Sole and others, 2013; Davison and others, 2020). This non-linear reaction to the influx of surface melt means that the effects of increasing amounts of meltwater, due to climate warming, are challenging to assess on inter-annual time scales. On shorter timescales, diurnal and multi-day variations in meltwater can affect glacier flow despite the presence of efficient drainage system (e.g. Schoof, 2010; Andrews and others, 2014).

Moon and others (2014) classified 55 marine-terminating glaciers, from the Greenland Ice Sheet, into three distinct types using TerraSAR-X-derived velocities from 2008 to 2013 at single points around 1 km from the termini. Following up on this study, Vijay and others (2019) used the PROMICE velocity dataset based on Sentinel-1 SAR data (Solgaard and others, 2021) to classify 45 marine-terminating outlet glaciers, many of the same glaciers as Moon and others (2014), at similar near-terminus points as the previous study. Flow speed variations of type-1 glaciers correlate well with calving front position changes and the change in the force balance at the front of the glacier dominates flow variations. Type-2 glaciers show increased flow speeds during summer following meltwater production, suggesting that increased water influx to the base is reducing the basal friction. Finally, type-3 glaciers slow down throughout most of the melt season to velocities lower than winter velocities. This is hypothesised to be due to the formation of an efficient drainage system: increasing meltwater volumes causes an efficient drainage system to evolve and thereby efficient drainage of the distributed water present at the base, resulting in low basal water pressure. Type-3 behaviour is observed at many SW Greenland glaciers (Vijay and others, 2021) for example at Kangiata

Nunaata Sermia (KNS, southwest Greenland, Ahlstrøm and others (2013); Davison and others (2020)) while type-2 behaviour prevails in the NW coast (Vijay and others, 2021) and for example Rink Isbrae (central western Greenland) in 2008–2013 (Ahlstrøm and others, 2013). However, the studies by Moon and others (2014); Vijay and others (2019); King and others (2020) also showed how glaciers change type from year to year and that many glaciers could not be classified.

The above mentioned studies classifying glaciers into distinct types had an ice-sheet wide focus, on a single point close to the terminus of the glaciers. An understanding of how the velocity variations vary with distance to the terminus could bring us closer to understanding what physical processes are causing the change in glacier type and/or that glaciers are not classifiable from year to year. Furthermore, ice surface flow speed derived from freely accessible satellite missions has a limitation in the temporal resolution. Flow speed reactions to changes in water influx to the base of fast-flowing marine-terminating glaciers have been shown to be within a day or down to ca 6.5 h at Helheim glacier (Andersen and others, 2010, 2011; Stevens and others, 2021), thus many details on processes related to short-term variations in surface meltwater flux remain unresolved.

Here we present a unique, satellite-derived, velocity dataset from Upernavik Isstrøm on the NW coast of Greenland in 2014 (Fig. 1). During a 68 d long campaign, around the end of the melt season in 2014, the COSMO-SkyMed satellites collected 15 SAR images with intervals between 1 and 8 d. From the SAR images, we derive 14 velocity maps enabling us to study spatial patterns of glacier flow speed changes on timescales similar to the reaction time of surface meltwater variability. While the studies of Moon and others (2014) and Vijay and others (2019) focused their analysis on a single point close to the terminus of a large number of glaciers, we extract the velocity variations at equidistant points, sampling every 1 km, along the centre flow lines up to around 20 km from the termini of the three neighbouring Upernavik glaciers. For simplicity, only points at 1, 10 and 20 km from the termini are compared with observations of surface meltwater production from the two on-ice Automatic Weather Stations (AWS) at Upernavik Isstrøm. From the analysis, we find that the three glaciers react promptly to changes in surface meltwater production. The velocity reaction to changes in surface meltwater production is comparable between the three glaciers above ca 6–10 km from the termini, but local conditions near the termini affect the velocity signal obscuring the meltwater-induced velocity variations.

2. Upernavik Isstrøm

The satellite observations presented in this paper cover a ca 2000 km^2 area at the front of Upernavik Isstrøm in NW Greenland (see Fig. 1) during 23 July to 28 September, 2014. To interpret the observations in the context of glacier geometry and dynamic regime, we briefly summarise the findings on the dynamical state of the Upernavik Isstrøm from Larsen and others (2016).

Upernavik Isstrøm consists of several outlet glaciers, all terminating in the same fjord: Upernavik Isfjord (Fig. 1). At present, three main outlet glaciers are flowing approximately from east to west identified here as UI-1, UI-2 and UI-3 (see Fig. 1). Just south of UI-3 there is a glacier with similar flow direction (UI-4 in Larsen and others (2016)) this glacier is not discussed here due to the slow flow and small size. Each of the calving fronts is ~5 km wide. The northernmost glacier, UI-1, is grounded at a water depth close to 1 km, the centre glacier, UI-2, is grounded at around 600 m, and the southernmost, UI-3, is grounded at ~500 m below sea level. The fjord is generally more shallow in the southern part. The northern part of the fjord is characterised by scattered icebergs and bergy-bits from UI-1. From UI-2 there are observations of large icebergs of up to 500 m across, an indication that part of the glacier tongue becomes afloat at the front. The southernmost glacier, UI-3, appears to be buttressed by a topographical high located at the grounding line, obstructing the free flow of icebergs that are calved off from the glacier.

Upernavik Isstrøm has undergone general retreat since 1849 (Weidick, 1958; Andresen and others, 2014). Between 2005 and 2008, UI-1 rapidly retreated 4 km inland as the calving front had moved into a topographically unstable position. The major retreat was followed by a doubling of ice flow speeds at the calving front of UI-1 within 1–2 years. From 2008 to 2014 the front remained relatively stable. A smaller retreat at UI-2 in 2009 of ~1 km also caused an increase in velocity by up to 80 % at the calving front within 4 years, where after UI-2 frontal position remained stable. While UI-1 and UI-2 have undergone rapid changes during the 2000s, the flow speed and terminus position of UI-3 have been remarkably stable. All three outlet glaciers showed only minor fluctuations in speed and calving front position in the years 2013–2014.

The studies by Moon and others (2014) and Vijay and others (2019) were not able to classify UI-1 as a distinct type based on observations near the calving front. UI-2 was unclassified by Moon and others (2014) based on observations from 2009 to 2013, but Vijay and others (2019) classified UI-2 as a type-1 glacier based on a correlation between calving front position and velocity variations in the period from 2015 to 2017. Velocity variations at UI-3 were observed to follow the meltwater production as a type-2 glacier from 2009 to 2013 (Moon and others, 2014) and for the period 2015–2017 UI-3 showed evidence of slow-down from early in the melt season as a type-3 glacier (Vijay and others, 2019).

3. Methods and data

3.1 COSMO-SkyMed satellite campaign and processing

COSMO-SkyMed is an Italian satellite constellation consisting of four identical satellites which were launched between 2007 and 2010. The mission is operated by the Agenzia Spaziale Italiana (ASI) and is funded by the Italian Ministry of Defence, and the Italian Ministry of Education, University, and Scientific Research. In the late summer of 2014, between 24 July and 2 October, 15 COSMO-SkyMed HIMAGE (3 × 3 m resolution) stripmap images of the area were acquired, utilising all four satellites in the constellation to achieve temporal baselines from 1 to 12 d. The campaign resulted in 14 pairs covering the period. Processing was carried out with the IPP (Interferometric Post Processing) ice velocity processor, developed by DTU Space and described in detail in Solgaard and others (2021). The processing retrieves local shifts by extracting corresponding patches in the two images and maximising the cross-correlation between the two patches. A patch size of 128 × 128 pixels (corresponding to ~300 × 300 m on the ground) was employed. Filtering of unreliable velocities was carried out by discarding measurements with a cross-correlation peak value below 0.05 and/or a signal-to-noise ratio of the peak estimate below 7, followed by a further outlier filtering based on local medians (Westerweel and Scarano, 2005). Velocity biases were calibrated using ground control points on stable rock, and the resulting velocity estimates were geocoded and projected onto x- and y-axes of the chosen map geometry, using the GIMP DEM (Howat and others, 2014) and assuming surface parallel flow. Error estimates on both latitudinal and longitudinal velocities are based on local standard deviations on the offset maps, scaled to velocity, and projected and geocoded in the same way as the velocity components.

Velocity maps represent the ice displacement between two SAR images with a specific time interval (called baselines in the

https://doi.org/10.1017/jog.2022.124 Published online by Cambridge University Press

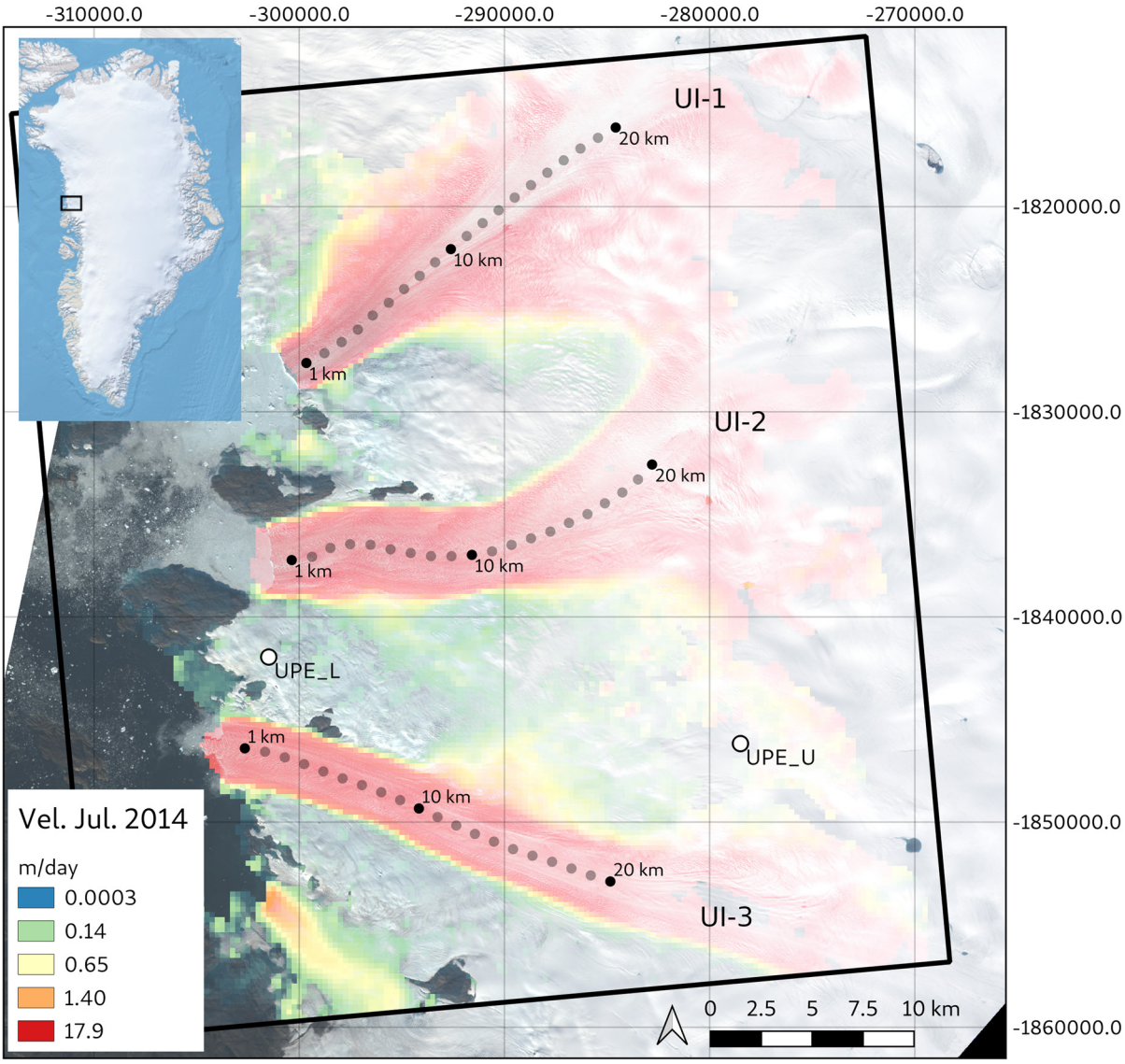


Fig. 1. Upernavik Isstrøm area seen from Landsat 8 (28/08/2014). Overlaid is a COSMO-SkyMed-derived velocity map from 23/07/2014. Black dots indicate data sampling points in km from the 2014 front corresponding to the locations presented in Figures 4–6. The three main outlet glaciers are designated UI-1, UI-2 and UI-3. Circles indicate the location of PROMICE weather stations. The black box outlines the COSMO-SkyMed coverage. Projected coordinate system EPSG:3413.

following). The baselines range between 1 and 8 d, in this case, most of the baselines are 8 and 4 d, while only one map has a 1- baseline. Thus every velocity map represents the total displacement between the two SAR images and variations on shorter timescales than the baselines are not represented in the data. When looking at velocity changes between two velocity maps the change in velocity could be a product of any combination of speed-up and slow-down events.

3.2 MEaSURES velocity maps

To put the short COSMO-SkyMed campaign into a seasonal context we use the TerraSAR-X-derived velocities from MEaSURES Greenland Ice Velocity Selected glacier velocity sites from inSAR (Joughin and others, 2021, 2010). An earlier version of these data was used to define glacier types in Moon and others (2014).

3.3 Sampling along centre flow lines

We extract velocity observations from the spatial data every 1 km along the centre flow lines. At each sampling point, we use the mean value of the velocity data within a 250 m radius. For simplicity, we focus our efforts on velocity sampled at distances of 1, 10, and 20 km from the front and refer to the full data set in the Supplementary Material when necessary (Figs S1, S2 and S3). Centre flow lines for the three glaciers UI-1, UI-2 and UI-3 are defined manually as the fastest flow axis based on a 2008–2009 winter velocity map (Joughin and others, 2010), the same centre flow lines as used in Larsen and others (2016).

3.4 Weather station data from PROMICE

We use in-situ observational data from the AWS provided by the Programme for Monitoring the Greenland Ice Sheet (PROMICE, doi: 10.22008/promice/data/aws. See also Fausto and others, 2021). The lower AWS, UPE_L is located very close to the coast at an elevation of 220 m above sea level (a.s.l.) ca 2 km from the margin. The upper AWS, UPE_U is located close to the equilibrium line at an elevation of 940 m a.s.l. ca 25 km from the margin.

We use ice ablation rates and positive degree days (PDD) to obtain information on meltwater production. Ablation rates are measured using a pressure transducer that records changes in ice surface elevation (Fausto and van As, 2012) and the PDD allow us to evaluate melt potential in the snow-covered periods,

https://doi.org/10.1017/jog.2022.124 Published online by Cambridge University Press

where ice melt rates are zero. The melt rates are determined by taking the day-to-day difference between the daily mean of the ice height measured by the pressure transducer. The PDD is calculated using hourly mean air temperature at an approximate height of 2.7 m above the ice surface in snow-free conditions, and lower when snow is present.

The transition between snowmelt and ice melt is determined by the shift in albedo to below 0.6 observed from radiometers on the AWSs (Supplementary Fig. 4).

3.5 Calving front positions

We manually digitised calving front positions on all available Landsat images (Landsat 7: doi: 10.5066/P9TU80IG, Landsat 8: doi: 10.5066/P975CC9B) during 2014 (Fig. 2). The calving fronts were distinguishable on all images.

3.6 Stress-coupling length

This study's focus on how the glacier flow reaction to changes in surface melt depends on the distance to the terminus, renders it necessary to understand how far calving-induced stress changes reach inland.

Stress-coupling length is the spatial scale over which stresses are transferred within glacier ice. The maximum theoretical stress coupling length is 4–10 times the ice thickness (Kamb and Echelmeyer, 1986). A study by Enderlin and others (2016) reached values for the ratio between stress-coupling length and ice thickness of 3.7 ± 1.7 and 4.2 ± 1.2 for the two marine-terminating glaciers Helheim glacier in SE Greenland and Columbia Glacier in Alaska, respectively. The thickness of three glaciers is obtained from BedMachine v3 (Morlighem and others, 2017) and sampled along the centre flow line at every 1 km similarly to the velocity (Fig. 3). Thickness is around 700–780 m near the termini and up to around 1.2 km at 20 km from the termini and the theoretical stress-coupling lengths vary between 1 km up to 11 km depending on the depth changes with distance to the termini (see Fig. 3 and Supplementary Table 1).

4. Results

Variation in the COSMO-SkyMed-derived velocities are evaluated at points every 1 km along the centre flow line. We present data from only three points along each centre flow line in Figures 4–6 at distances of 1, 10 and 20 km from the front (panels A, B and C respectively). Velocity variations at all the points can be found in the Supplementary Figures 1–3. The relatively short COSMO-SkyMed campaign is put into context to the annual flow speed variation from the TerraSAR-X-derived velocities (Figs 4–6). Absolute velocities are consistent when taking into account the velocity maps covering different periods. The only exception is near the front of UI-1 where the two velocity datasets are shifted by ca 0.5 m d^{-1} (Fig. 4). This inconsistency results from the difference in local slope of the two digital elevation models used. The COSMO-SkyMed data were processed using a modified version of the GIMP DEM v1 (Howat and others, 2014), downsampled to 500 m resolution and the TerraSAR-X data are-processed using the 90 m GIMP DEM v1, this difference will particularly be evident in areas with large elevation differences or changes in terminus position (MEaSUREs Greenland Ice Velocity: Selected Glacier Site Velocity Maps from InSAR, Version 4 User Guide (https://nsidc.org/data/nsidc-0481/versions/4)).

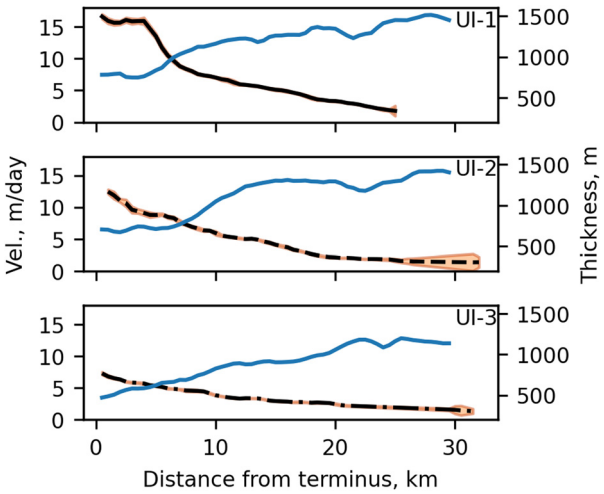


Fig. 2. The COSMO-SkyMed-derived velocity from 23/07/2014 (dashed black lines, with error estimate in shaded orange) plotted with glacier ice thickness from BedMachine v4 (Morlighem and others, 2017) (blue lines), along the centre flow lines of UI-1 (top panel), UI-2 (middle panel) and UI-3 (lower panel).

4.1 Melt conditions

On Figures 4–6, panel D shows the same observations of PDD and ice melt rates at the two on-ice PROMICE weather stations. The melt season starts (mostly snow melt) at the beginning of June, and ice melt starts around 15 June at UPE_L and around 28 June at UPE_U. Ice melt rates are mostly above 5 cm d^{-1} at both UPE_U and UPE_L until around 5 August when melt rates at UPE_U start a decreasing trend towards zero on 16 August, while remaining stable at UPE_L. In the period 17–22 August melt rates at UPE_U are again between 4 to 5 cm d^{-1} and comparable to UPE_L. On 23 August melt rates drop to zero at UPE_U and start a decreasing trend at UPE_L. In the last week of August melt conditions re-emerge at UPE_U for 4 d, and again on 6 to 7 September, and on 20 September melt conditions cease. Most relevant to this study is the upper station UPE_U (blue curve in panel D in Figs 4–6) due to the location close to the equilibrium line.

4.2 UI-1

The northernmost glacier, UI-1, is the fastest of the three glaciers with a mean velocity of 15.4 m d^{-1} close to the calving front (Fig. 3 and Table 1). The COSMO-SkyMed-derived velocities vary in total between 5 and 6 % (Table 1) and the calving front remains stable throughout 2014 (Fig. 2).

At UI-1 (Fig. 4), the TerraSAR-X-derived velocities indicate a velocity peak around mid-July at both 1 and 10 km from the terminus (panels A and B in Fig. 4), ca 1–2 weeks before the melt-peak and middle of melt-season, while at a distance of 20 km from the terminus (panel C in Fig. 4) velocities peak at the beginning of June, coinciding with the beginning of melt. The COSMO-SkyMed data series starts just after the seasonal velocity peak, with a slow-down around 26 July at all three locations. During the 3 weeks following this slow-down, velocities are generally increasing at 1 and 10 km while melt rates are decreasing or stagnant (at UPE_U and UPE_L respectively). In contrast, at 20 km velocities are stagnant or slightly decreasing for the same period. Upstream of 5 km from the terminus, we observed a speed-up between 15 and 23 August (Fig. 4 and Supplementary Fig. 4). This speed-up, of 1.7 and 3.3 % increase in velocity at 10 and 20 km respectively (Table 1) coincides with increased melt rates at UPE_U on 16 and 17 August. This late-season speed-up ends with a second significant slow-down reducing velocity between 3 and 4 % from 23 August, bringing the COSMO-SkyMed-derived velocities to the lowest recorded value in the dataset around the same day as melt rates go to zero at UPE_U.

https://doi.org/10.1017/jog.2022.124 Published online by Cambridge University Press

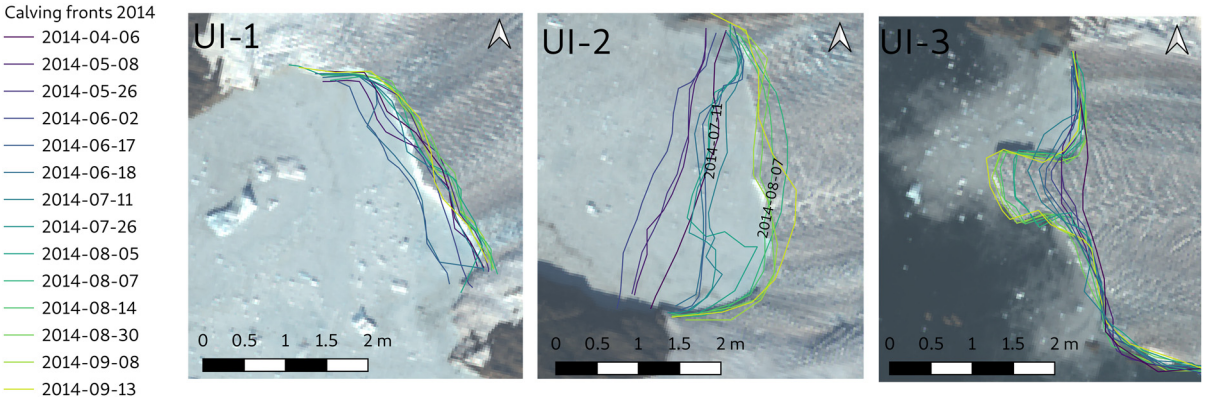


Fig. 3. Calving front positions of UI-1, UI-2 and UI-3. Full coloured lines are digitised manually for this study from all available and cloud-free Landsat images in 2014.

Subsequent variations in velocity from the end of August to the first week of September coincide with the re-occurrence of melt conditions at UPE_U from 26 August to 1 September. From 15 September and to the end of the record, we see a slight increasing trend in velocities at 1 and 10 km.

4.3 UI-2

The central glacier, UI-2, has an average velocity of around 12.5 m d^{-1} close to the calving front (Fig. 3 and Table 1). The COSMO-SkyMed-derived velocities vary in total between 9 and 13 % (Table 1) and the calving front is retreating ~1.5–2 km during 2014 (Fig. 3 and Supplementary Fig. 5).

The TerraSAR-X-derived velocity at UI-2 (Fig. 5) shows an increasing trend throughout the melt season at the point 1 km from the terminus (panel A in Fig. 5). At 10 km from the terminus (panel B in Fig. 5), velocities peak around mid-July while at a distance of 20 km from the terminus (panel C in Fig. 5) velocities are relatively high from the beginning of the record until around 26 July. The COSMO-SkyMed-derived velocity variations resemble the variations at UI-1 starting with a slow-down around 26 July, followed by 3 weeks of increasing

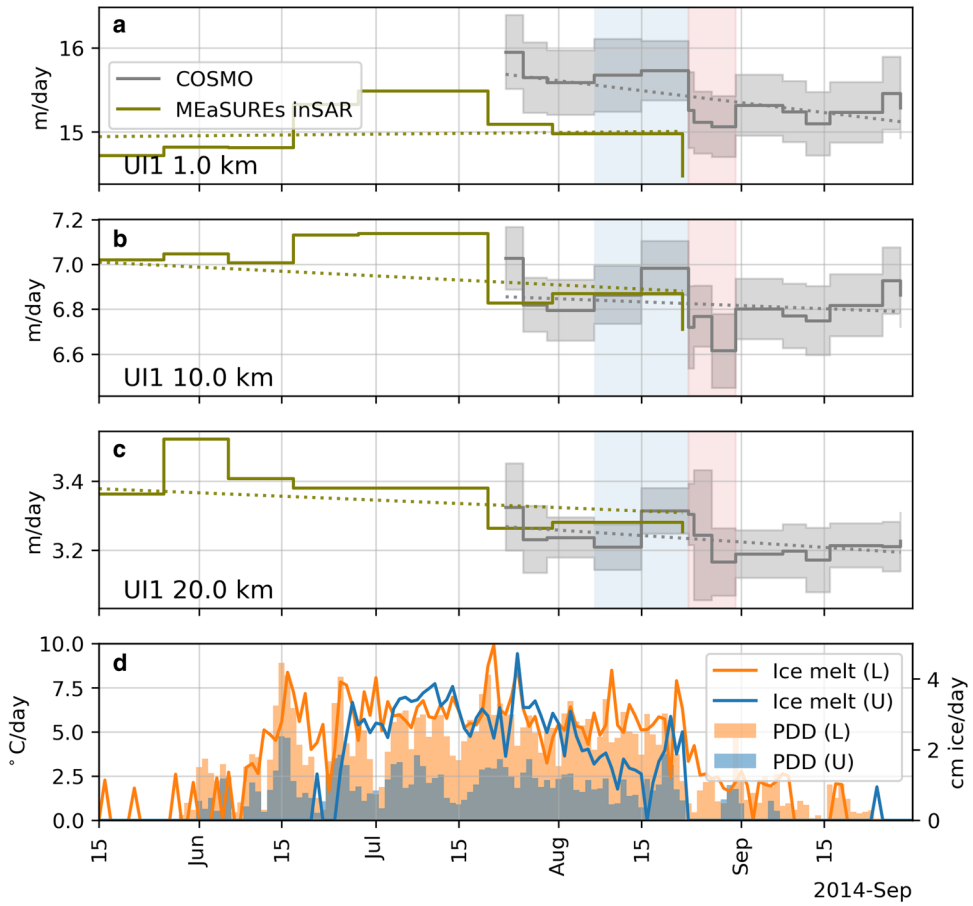


Fig. 4. UI-1: Velocity at three points ~1 km (panel A), 10 km (panel B) and 20 km (panel C) from the terminus of UI-1 and the observed ice ablation. The gray line is the COSMO-SkyMed-derived velocities including error estimates in gray bars, green line is the MEaSUREs inSAR data for reference. Dotted lines are the weighted trends within each velocity dataset and the shaded blue and red areas mark the Peak and Drop periods defined in Table 1. Panel D shows air temperature and derived positive degree days (PDD) from the PROMICE automatic weather stations UPE_U and UPE_L.

https://doi.org/10.1017/jog.2022.124 Published online by Cambridge University Press

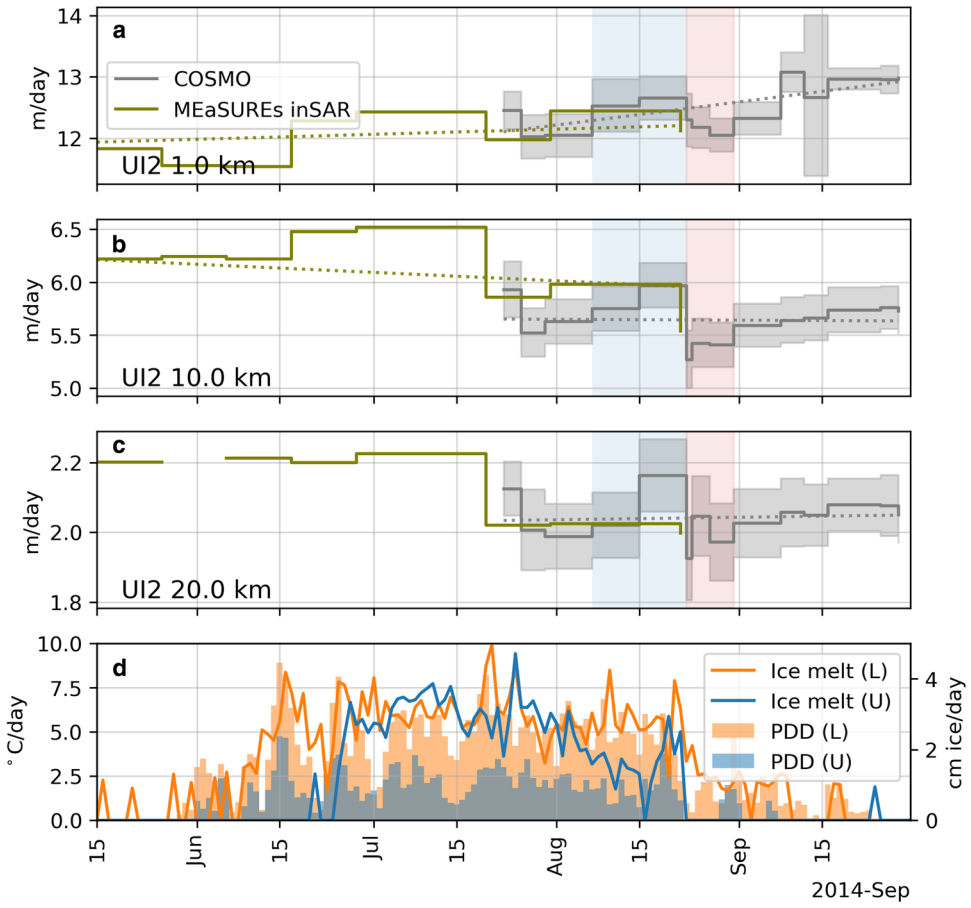


Fig. 5. UI-2: Velocity at three points ~1 km (panel A), 10 km (panel B) and 20 km (panel C) from the terminus of UI-2 and the observed ice ablation. The gray line is the COSMO-SkyMed-derived velocities including error estimates in gray bars, green line is the MEaSUREs inSAR data for reference. Dotted lines are the weighted trends within each velocity dataset and the shaded blue and red areas mark the Peak and Drop periods defined in Table 1. Panel D shows air temperature and derived positive degree days (PDD) from the PROMICE automatic weather stations UPE_U and UPE_L.

trends at 1 and 10 km and close to stagnant at 20 km while the melt rate is decreasing and stagnant at UPE_U and UPE_L respectively. Between 15 and 22 August, melt rates increase again at UPE_U and we observe a clear speed-up of 3.8 and 7.0 % increase in velocity at 10 and 20 km respectively (Table 1). This speed-up is less pronounced at 1 km with only 1 % increase in velocity (Table 1). Similar to UI-1 a significant slow-down, reducing velocities by 4–10 % (Table 1), occurs after 23 August when melt stops at UPE_U. At UI-2 this second slow-down brings velocities to a minimum at 10 and 20 km, however, velocities do not reach their minimum at 1 km (Fig. 4). The general acceleration over the entire observational period extends to around 6 km from the front (Supplementary Fig. 2).

4.4 UI-3

UI-3 is the slowest flowing glacier of the three, with a velocity close to 6 m d^{-1} at 1 km from the terminus (Fig. 3 and Table 1). The COSMO-SkyMed-derived velocities vary in total between 13 and 22 % (Table 1). The calving front is dominated by an island just at the centre flow ling extending up to 1.5 km between 6 April and 13 September (Fig. 2), on both the northern and southern side of the outcrop, the calving front position remained stable in 2014.

The TerraSAR-X-derived velocities show a peak around mid-July 1 km from the terminus (panel A in Fig. 6), at 10 km the velocity peaks a few weeks earlier around 20 June (panel B in Fig. 6) and at 20 km the peak occurs around the initiation of melt (panel C in Fig. 6). Similar to UI-1 and UI-2 the COSMO-SkyMed-derived velocities slow down around 26 July at 1 and 10 km from the terminus. In contrast to UI-1 and UI-2, the velocities are stagnant or decreasing in the following weeks at all their points. Between 15 and 22 August, speed-up occurs with velocities increasing by 3 and 7 % at 10 and 20 km respectively (Table 1) in the same period where increased melt rates are observed. This late-season speed-up is not seen from the terminus and 7 km upstream of UI-3 terminus (Supplementary Fig. 3). On 23 August, when melt rates drop to zero at UPE_U, we observe a following slow-down lowering velocities by around 10 % (Table 1), bringing UI-3 velocities to the lowest value in the dataset at all three points. This velocity minimum is followed by a slow speed-up throughout September.

5. Discussion

We observe a correlation between ice velocity changes and variability in surface melt on timescales of days to weeks, and that the ice velocity response depends on the distance to the terminus. The analysis below, furthermore, exemplifies the different timescales on which glacier flow responds to meltwater production.

5.1 Early melt season response

Generally, in the early melt season (TerraSAR-X data), the velocities peak earlier with increasing distance from the terminus. The early speed-up response to the initiation of surface melt at 20 km from the termini at UI-1 and UI-3 indicates that the subglacial hydrology system is overwhelmed at the onset of surface melt,

https://doi.org/10.1017/jog.2022.124 Published online by Cambridge University Press

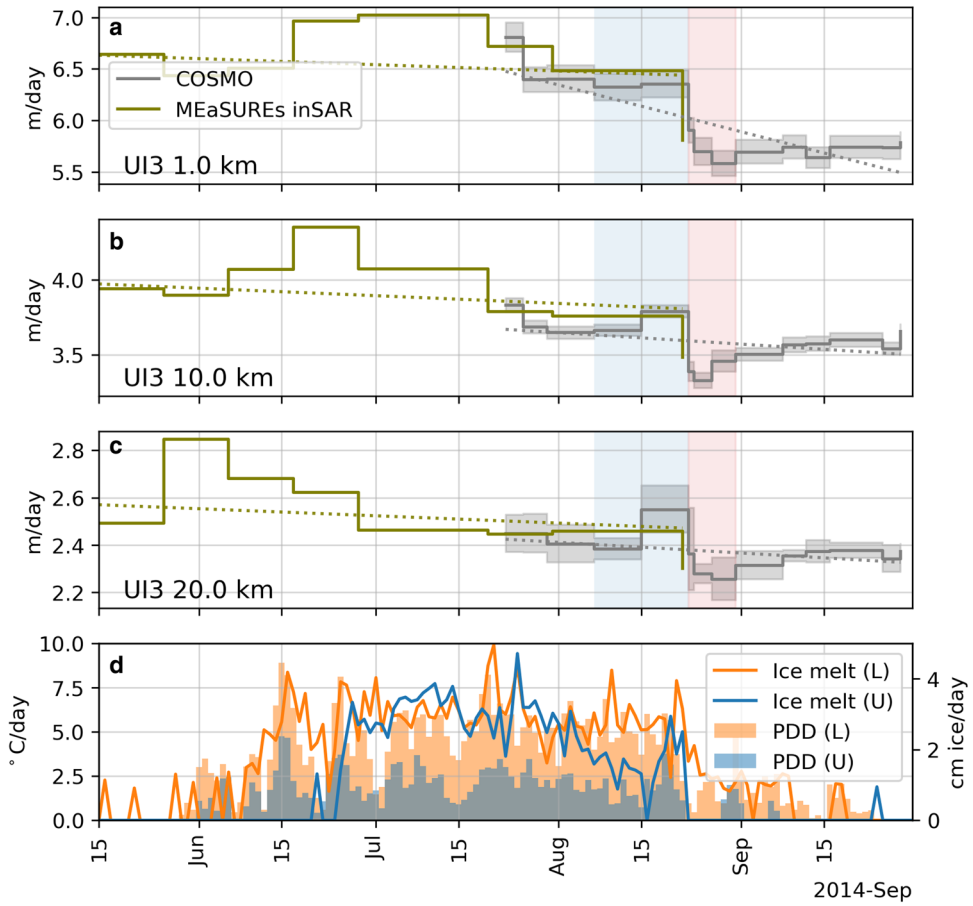


Fig. 6. UI-3: Velocity at three points ~1 km (panel A), 10 km (panel B) and 20 km (panel C) from the terminus of UI-3 and the observed ice ablation. The gray line is the COSMO-SkyMed-derived velocities including error estimates in gray bars, green line is the MEaSUREs inSAR data for reference. Dotted lines are the weighted trends within each velocity dataset and the shaded blue and red areas mark the Peak and Drop periods defined in Table 1. Panel D shows air temperature and derived positive degree days (PDD) from the PROMICE automatic weather stations UPE_U and UPE_L.

and friction is rapidly reduced because the subglacial hydrology system can only accommodate relatively small volumes of water (Bartholomew and others, 2010; Hoffman and Price, 2014). This early speed-up at a distance of 20 km from the terminus is not observed at UI-2, where the onset of melt coincides with a data gap. The data gap covers exactly the period where a peak is seen at UI-1 and UI-3 thus an early speed-up 20 km upstream from terminus at UI-2 cannot be either confirmed or ruled out. The early speed-up decreased again within 2–3 weeks indicating that drainage channels evolved and adapted to the increased amount of water within this period. Furthermore, flow speeds at 20 km showed no reaction to the increased melt rates around 15 June, implying that the change in water volume reaching the bed is relatively low compared to volume of water already present. At the points around 1 and 10 km from termini at UI-1, UI-2 and UI-3 velocities peak during the first weeks of July, this is 3–4 weeks later than the early velocity peaks at 20 km, and coinciding with increased melt rates due to the transition between snow and ice melt. At these distances, closer to the termini, change in flow conditions due to the early melt period at the beginning of June is not visible in the velocity data. Thus, we infer that a flow speed response in this zone requires a larger total volume of water. We suggest this relates to the existing water pressure and drainage systems before the onset of melt. The closer to the terminus of a glacier, the faster the flow speed and hence also basal meltwater formation resulting in more water being present year-round (Karlsson and others, 2021).

Table 1. COSMO-SkyMed-derived velocity data statistics

	UI-1			UI-2			UI-3		
	1 km	10 km	20 km	1 km	10 km	20 km	1 km	10 km	20 km
Mean (m d^{-1})	15.40	6.82	3.23	12.51	5.64	2.04	5.98	3.59	2.38
Range (m d^{-1})	0.88	0.41	0.16	1.05	0.70	0.24	1.22	0.50	0.29
Range (%)	5.87	6.23	5.00	8.75	13.27	12.36	21.95	15.11	13.04
Peak (m d^{-1})	0.05	0.12	0.10	0.13	0.22	0.14	0.03	0.13	0.17
Peak (%)	0.35	1.74	3.25	1.01	3.82	7.04	0.49	3.42	6.96
Drop (m d^{-1})	0.62	0.29	0.10	0.52	0.57	0.16	0.68	0.40	0.27
Drop (%)	3.94	4.14	2.95	4.13	9.55	7.53	10.77	10.48	10.66

Mean refers to the mean of all observed velocities at a given location. Range refers to the range between the minimum and maximum recorded velocity at a given location. Peak refers to the difference between the velocity between 7 and 15 August and the velocity between 15 and 23 August; the percentage change is relative to the velocity between 7 and 15 August. Drop refers to the difference between the velocity between 15 and 23 August and the weighted mean velocity between 23 and 31 August; the percentage change is relative to the velocity between 15 and 23 August.

5.2 Late melt season response

The COSMO-SkyMed-derived velocities showed two main events, in the late melt season, which will be the focus of the discussion: the Peak relating to the increased flow speeds between 15 and 22 August, and the Drop referring to the slow-down around August 23 (Table 1).

The Peak in the COSMO-SkyMed-derived velocities is a period with increased flow speeds between 15 and 22 August. The magnitude of this speed-up relative to the local mean velocity increases with distance from the termini (Figs 4–6 and Table 1) and at UI-3 it is not evident downstream of 7 km from the

https://doi.org/10.1017/jog.2022.124 Published online by Cambridge University Press

terminus (Supplementary Fig. S3). The Peak occurring in the late melt-season coincides with a few days of increased surface meltwater production after a week of reduced melting (blue curve in panel D, Figs 4–6). The speed-up suggests that the efficiency of the subglacial hydrology system had deteriorated, as a result of the reduced melt rates during the period 1–15 August. The relative magnitude of the Peak increases with distance to the front (Table 1) which indicates that the change in surface-derived melt water has a relatively higher importance in upstream areas. This could relate to the decreasing amount of basal water available upstream, which makes the ratio between meltwater volumes from the surface relatively larger compared to the basal water volumes. When this speed-up is not evident close to the terminus of UI-3, it could thus relate to a slower closure rate of the drainage system in this area.

The Drop in the COSMO-SkyMed-derived velocities is the slow-down taking place around 23 August. The resolution of the data does not allow an exact determination of the timing of the slow-down, however, the slow-down event is likely closely linked to the drop in meltwater production between August 23 and 24. The COSMO-SkyMed-derived velocity maps capture the low velocities after August 23 with high temporal resolution (1–4 d baselines). These low velocities are observed at all observation points starting from the same day as meltwater production abruptly drops (Figs 4–6 and Supplementary Figs S1–3). A short reaction time between a change in local surface meltwater and the glacier flow reaction time was observed from the GPS study at Helheim glacier, where a reaction time of down to 6.5 h was found up to 35 km upstream from the margin with no evidence of any change in reaction time with distance to the margin (Stevens and others, 2021). While the timing of the slow-down cannot be determined precisely, we hypothesise that an abrupt slow-down caused by the cut-off of surface meltwater similar to that experienced at Helheim glacier occurred at Upernavik Isstrøm on 23–24 August. The fact that the majority of the velocity maps have baselines of 4–8 d means that we cannot exclude that similar, fast-reacting slow-down events occurred at other times.

5.3 Response to calving events

While the calving fronts of UI-1 remained stable throughout 2014, UI-2 experienced a calving front retreat in June and July. On 2 June the calving front advanced to its maximum position, and on 7 August the margin retreated to the minimum position (Fig. 3 and Supplementary Fig. S5). A calving-induced acceleration in flow speeds can be seen up to around 6 km from the terminus at UI-2 throughout the observational period (Fig. 5 and Supplementary Fig. S2). With ice thickness around 740 m results in a stress-coupling length around eight times the ice thickness, which is slightly larger than 3.7 ± 1.7 H and 4.2 ± 1.2 H found for Helheim Gletsjer (SE Greenland) and Columbia (Alaska) glacier but within the theoretical maximum of 10 H (Kamb and Echelmeyer, 1986). The response from the terminus up to around 6 km corresponds to the type-1 glacier identified by Moon and others (2014), however, above 6 km a more direct relationship between ice velocities and surface meltwater emerges, indicating a type-2 glacier. From this, we argue that the classification depends on the distance to the calving front. Furthermore, we suggest that theoretical values of stress-coupling lengths can be used to ensure analysis of velocity variations are not dominated by calving-induced acceleration.

We did not observe any similar relationships between calving events and glacier flow speed at UI-3. At UI-3 an advance occurs on a limited outcrop of the calving front during the observational period, without having a similar effect on flow speed as on UI-2 (Fig. 6). We believe that this relates to the geometry of UI-3, where the limited spatial extent of the outcrop is likely linked to basal topography.

6. Conclusion

A COSMO-SkyMed satellite campaign around the end of melt in 2014, focusing on Upernavik Isstrøm, resulted in 14 velocity maps with a higher spatial and temporal resolution than any other satellite-derived velocity product.

Here, we present changes in surface meltwater volumes and corresponding changes in surface velocity at points at 1, 10 and 20 km from the termini of the three marine-terminating glaciers UI-1, UI-2 and UI-3. The analysis revealed that with increasing distance to the termini, velocity peaks on timescales of days to weeks in occurred earlier and with (relative) larger increase. This is observed early in the melt season in the TerraSAR-X data and later in the season in the COSMO-SkyMed data. The velocity response dependence on the distance to the terminus is explained by the relative difference between changes in the surface-derived water volumes compared to the water volumes present at the base.

A retreat of the terminus of UI-2 in the first half of 2014 caused an acceleration of UI-2 that dominated the velocity pattern. This calving-induced acceleration was clear up to a distance of around 6 km from the terminus, and we suggest that using theoretical stress-coupling values can be used to identify velocity response to surface meltwater variations, despite calving-induced acceleration.

Our analysis demonstrates how high-resolution satellite-derived velocity observations can identify important processes controlling outlet glacier response to surface melt. The variations in surface velocity at Upernavik outlet glaciers in 2014 depended on the availability of surface meltwater, the distance to the front as well as calving front retreat. Our results demonstrate that a complete understanding of subglacial hydrologic conditions requires information on frontal and surface processes as well as local factors such as basal melt rates. Future detailed studies on similar timescales of individual marine-terminating outlet glaciers may reveal detailed information on why glaciers react differently to similar forcing.

Supplementary material. The supplementary material for this article can be found at https://doi.org/10.1017/jog.2022.124

Data availability. The COSMO-SkyMed-derived velocity data are available on the GEUS dataverse: https://doi.org/10.22008/FK2/IH3JAS

Acknowledgements. This is a publication within the Nordic Centre of Excellence SVALI, 'Stability and Variations of Arctic Land Ice' funded by the Nordic Top-level Research Initiative (TRI). We thank Christine Dow and Anne M. Solgaard for their useful feedback. Our gratitude also goes to Twila Moon and an anonymous reviewer for the very useful and constructive feedback, the comments significantly improved the manuscript. The professional handling by Editor Bea Csatho is also deeply appreciated. PLL gratefully acknowledges the contributions of the Aarhus University Interdisciplinary Centre for Climate Change (iClimate, Aarhus University).

References

Ahlstrøm AP and 13 others (2013) Seasonal velocities of eight major marine-terminating outlet glaciers of the Greenland ice sheet from continuous in situ GPS instruments. *Earth System Science Data* **5**(2), 277–287. doi:10.5194/essd-5-277-2013

Andersen ML and 14 others (2010) Spatial and temporal melt variability at Helheim Glacier, East Greenland, and its effect on ice dynamics. *Journal of Geophysical Research: Earth Surface* **115**(4), 1–18. doi:10.1029/2010JF001760

Andersen ML, Nettles M, Elosegui P, Larsen TB, Hamilton GS and Stearns LA (2011) Quantitative estimates of velocity sensitivity to surface melt

variations at a large Greenland outlet glacier. *Journal of Glaciology* **57**(204), 609–620. doi:10.3189/002214311797409785

Andresen CS, Kjeldsen KK, Harden B, Nørgaard-Pedersen N and Kjær KH (2014) Outlet glacier dynamics and bathymetry at Upernavik. *GEUS Bulletin* **31**(2014), 81–84.

Andrews LC and 7 others (2014) Direct observations of evolving subglacial drainage beneath the Greenland Ice Sheet. *Nature* **514**(7520), 80–83. doi:10.1038/nature13796

Bartholomew I, Nienow P, Mair D, Hubbard A, King MA and Sole A (2010) Seasonal evolution of subglacial drainage and acceleration in a Greenland outlet glacier. *Nature Geoscience* **3**(6), 408–411. doi:10.1038/ngeo863

Catania GA, Stearns LA, Moon TA, Enderlin EM and Jackson RH (2020) Future evolution of Greenland's marine-terminating outlet glaciers. *Journal of Geophysical Research: Earth Surface* **125**(2), 1–28. doi:10.1029/2018JF004873

Cuffey K and Paterson WSB (2010) *The Physics of Glaciers*. 4th Edn. Elsevier.

Davison BJ and 6 others (2020) Subglacial drainage evolution modulates seasonal ice flow variability of three tidewater glaciers in Southwest Greenland. *Journal of Geophysical Research: Earth Surface* **125**(9), 005492. doi:10.1029/2019JF005492

Enderlin EM, Hamilton GS, O'Neel S, Bartholomaus TC, Morlighem M and Holt JW (2016) An empirical approach for estimating stress-coupling lengths for marine-terminating glaciers. *Frontiers in Earth Science* **4**, 00104. doi:10.3389/feart.2016.00104

Fausto R and 16 others (2021) Programme for Monitoring of the Greenland Ice Sheet (PROMICE) automatic weather station data. *Earth System Science Data* **13**, 3819–3845. doi:10.5194/essd-13-3819-2021

Fausto RS and van As D (2012) Ablation observations for 2008–2011 from the Programme for Monitoring of the Greenland Ice Sheet (PROMICE). *Geological Survey of Denmark and Greenland, Bulletin* **26**, 73–76.

Hoffman M and Price S (2014) Feedbacks between coupled subglacial hydrology and glacier dynamics. *Journal of Geophysical Research: Earth Surface* **119**(3), 414–436. doi:10.1002/2013JF002943

Howat IM, Negrete A and Smith BE (2014) The Greenland Ice Mapping Project (GIMP) land classification and surface elevation data sets. *The Cryosphere* **8**(4), 1509–1518. doi:10.5194/tc-8-1509-2014

The IMBIE Team (2020) Mass balance of the Greenland Ice Sheet from 1992 to 2018. *Nature* **579**, 233–239. doi:10.1038/s41586-019-1855-2.

Joughin I, Howat I, Smith B and Scambos T (2021) MEaSUREs Greenland ice velocity: selected glacier site velocity maps from inSAR, version 4. Subset W72.90N. Boulder, Colorado USA. *NASA National Snow and Ice Data Center Distributed Active Archive Center*. https://nsidc.org/data/nsidc-0481/versions/4 Accessed March 16, 2022.

Joughin IR, Smith BE, Howat IM, Scambos T and Moon T (2010) Greenland flow variability from ice-sheet-wide velocity mapping. *Journal of Glaciology* **56**(197), 415–430. doi:10.3189/002214310792447734

Kamb B and Echelmeyer KA (1986) Stress-gradient coupling in glacier flow: I. Longitudinal averaging of the influence of ice thickness and surface slope. *Journal of Glaciology* **32**, 267–284.

Karlsson NB and 13 others (2021) A first constraint on basal melt-water production of the Greenland Ice Sheet. *Nature Communications* **12**(1), 1–10. doi:10.1038/s41467-021-23739-z

King MD and 8 others (2020) Dynamic ice loss from the Greenland Ice Sheet driven by sustained glacier retreat. *Communications Earth & Environment* **1** (1), 1–7. doi:10.1038/s43247-020-0001-2

Larsen SH, Khan SA, Ahlstrøm AP, Hvidberg CS, Willis MJ and Andersen SB (2016) Increased mass loss and asynchronous behavior of marine-terminating outlet glaciers at Upernavik Isstrøm, NW Greenland. *Journal of Geophysical Research: Earth Surface* **121**(2), 241–256. doi:10.1002/2015JF003507

Moon T and 6 others (2014) Distinct patterns of seasonal Greenland glacier velocity. *Geophysical Research Letters* **41**(20), 7209–7216. doi: 10.1002/2014GL061836.Received

Morlighem M and 25 others (2017) BedMachine v3: complete bed topography and ocean bathymetry mapping of greenland from multibeam echo sounding combined with mass conservation. *Geophysical Research Letters* **44**(21), 11051–11061. doi:10.1002/2017GL074954

Mouginot J and 8 others (2019) Forty-six years of Greenland Ice Sheet mass balance from 1972 to 2018. *Proceedings of the National Academy of Sciences of the USA* **116**(19), 9239–9244. doi: 10.1073/pnas.1904242116

Rathmann NM and 7 others (2017) Highly temporally resolved response to seasonal surface melt of the Zachariae and 79N outlet glaciers in northeast Greenland. *Geophysical Research Letters* **44**(19), 9805–9814. doi:10.1002/2017GL074368

Schoof C (2010) Ice-sheet acceleration driven by melt supply variability. *Nature* **468**(7325), 803–806. doi:10.1038/nature09618

Sole A and 6 others (2011) Seasonal speedup of a Greenland marine-terminating outlet glacier forced by surface melt-induced changes in subglacial hydrology. *Journal of Geophysical Research* **116**(F3), F03014. doi: 10.1029/2010JF001948

Sole A and 12 others (2013) Winter motion mediates dynamic response of the Greenland Ice Sheet to warmer summers. *Geophysical Research Letters* **40** (15), 3940–3944. doi: 10.1002/grl.50764

Solgaard A and 12 others (2021) Greenland ice velocity maps from the PROMICE project. *Earth System Science Data* **13**(7), 3491–3512. doi:10.5194/essd-13-3491-2021

Stevens LA and 6 others (2021) Helheim Glacier diurnal velocity fluctuations driven by surface melt forcing. *Journal of Glaciology* **68**(267), 77–89. doi:10.1017/jog.2021.74

van der Veen CJ, Plummer JC and Stearns LA (2011) Controls on the recent speed-up of Jakobshavn Isbræ West Greenland. *Journal of Glaciology* **57** (204), 770–782. doi:10.3189/002214311797409776

Vijay S, Khan SA, Kusk A, Solgaard AM, Moon T and Bjørk AA (2019) Resolving seasonal ice velocity of 45 Greenlandic glaciers with very high temporal details. *Geophysical Research Letters* **46**(3), 1485–1495. doi:10.1029/2018GL081503

Vijay S, King MD, Howat IM, Solgaard AM, Khan SA and Noël B (2021) Greenland ice-sheet wide glacier classification based on two distinct seasonal ice velocity behaviors. *Journal of Glaciology* **67**(266), 1241–1248. doi:10.1017/jog.2021.89

Weidick A (1958) Frontal variations at Upernaviks Isstrøm in the last 100 Years. *Meddelelser fra dansk geologisk forening/Bulletin of the Geological Society of Denmark*, Vol. 14.

Westerweel J and Scarano F (2005) Universal outlier detection for PIV data. *Experiments in Fluids* **6**(39), 1096–1100. doi:10.1007/s00348-005-0016-6

https://doi.org/10.1017/jog.2022.124 Published online by Cambridge University Press